



Cite this: *RSC Adv.*, 2023, 13, 13809

Solvothermal synthesis of hair-like carbon nanotubes onto sub-micron-sized spherical metal oxide catalyst cores†

Kazuya Kobiro,^a  ^{ab} Hinako Kimura,^a Saki Hirose,^a Makoto Kinjo^a and Hiroshi Furuta  ^{ac}

Long- and uniform-length, and high-density hair-like carbon nanotubes (CNTs) were produced by CNT growth on sub-micron-sized spherical catalyst supports. The nanosized catalysts (FeO_x , CoO_x , and NiO_x) that were supported in/on the sub-micron-sized spherical metal oxides (TiO_2 , ZrO_2 , SnO_2 , and CeO_2) were prepared *via* one-step solvothermal and/or two-step impregnation methods. The nanosized catalysts supported in/on the spherical metal oxide supports were converted into CNT conjugates with the CNT-hair morphology *via* a chemical thermal vapor deposition technique using ethyne gas as a carbon source; the CNTs grew on the central spherical metal oxide core under the base growth process conditions. Among the many types of candidate spherical catalyst materials, the combination of FeO_x as a catalyst for CNT growth and ZrO_2 as a support led to the best growth of CNT-hair under the reaction conditions, which included a temperature of 730 °C, pressure of 65 Pa, a 10 sccm ethyne gas flow, and a reaction time of 10 s. The CNTs consisted of five-to-eight-layered multi-wall structures with lengths of approximately 3 μm . The CNT-hair that was obtained using the solvothermally embedded catalyst showed higher crystallinity and was dense, thick, and straight, while the corresponding CNT-hair obtained using the impregnated catalyst was slightly sparse, thin, and curly. A unique layer structure constructed using large quantities of uniform CNT-hair, including multiple CNT yarns similar to fuzzy balls or cotton candies, was assembled. The CNT-hair conjugate, specifically constructed in a layer structure with core $\text{FeO}_x/\text{ZrO}_2$ catalysts and tangled CNT yarns, had an appearance similar to frog eggs. Therefore, we successfully prepared suitable catalysts for CNT-hair production and fabricated a layer structure consisting of large numbers of CNT-hair conjugates. The unique structures are expected as a new metamaterial with intriguing physical properties, including isotropic absorption of polarized light and electromagnetic waves.

Received 5th February 2023
Accepted 28th April 2023

DOI: 10.1039/d3ra00770g

rsc.li/rsc-advances

Introduction

Carbon nanotubes (CNTs) have attracted researchers' interest because of their unique electrical, thermal, and mechanical properties since they were first reported by Iijima.¹ A wide variety of CNT-based applications have been reported that use their specific properties in transistors, chemical sensors, thermal absorbers, composites with carbon nanotubes, loudspeakers, and wires for space-elevators. Both quality control and

mass production of these CNTs are desired for further development of future applications based on CNTs.

Commercially available CNTs such as HiPCo and CoMoCAT are produced *via* gas-phase synthesis using catalytic thermal chemical vapor deposition (CVD). In these processes, residual metal catalysts remain in the bodies of the nanotubes, which can cause their electrical, thermal, and mechanical properties to degrade. A relatively new method to accomplish high-purity fabrication of CNTs was investigated using catalytic thermal CVD on substrates, by which CNTs are grown with high-area density and uniform lengths on catalysts on the substrates. High-quality CNTs with low amounts of residual catalytic metals in the CNT bodies are expected to be produced by the catalytic thermal CVD process on the substrates.

Increasing the mass of CNT production in a single batch during high-quality thermal CVD growth on flat substrates is still challenging. Noda *et al.* reported higher mass production of CNTs on 0.1 mm-sized Al_2O_3 beads using a thermal CVD process that combined a fluidized-bed method with catalytic

^aGraduate School of Engineering, Kochi University of Technology, 185 Miyakouchi, Tosayamada, Kochi 782-8502, Japan. E-mail: kobiro.kazuya@kochi-tech.ac.jp; furuta.hiroshi@kochi-tech.ac.jp

^bCenter for Structural Nanochemistry, Research Institute, Kochi University of Technology, 185 Miyakouchi, Tosayamada, Kochi 782-8502, Japan

^cCenter for Nanotechnology, Research Institute, Kochi University of Technology, 185 Miyakouchi, Tosayamada, Kochi 782-8502, Japan

† Electronic supplementary information (ESI) available. See DOI: <https://doi.org/10.1039/d3ra00770g>



thermal CVD by increasing the surface area of the substrates.^{2,3} Verpillere *et al.* reported the smallest diameter for the spherical substrate to increase the surface area of the substrates,⁴ but the uniformity of the diameter of the spherical substrate was not investigated.

Vertically aligned high-areal density CNT films were grown on substrates to a uniform length to produce so-called CNT forests, which opened up a wide variety of new applications for CNTs in the electrical, mechanical, and optical fields, including field emitters, electrode structures for secondary batteries, and metamaterials. We have previously reported uniform and high-density growth of CNT forests using thin film metal catalysts followed by thermal CVD using carbon gas sources. The height of the CNTs was controlled from an optical wavelength scale of <1 μm to a mechanical scale of 250 μm in length *via* pulse gas source control using an automated gas bulb.^{5,6} Optical metamaterial features including resonance absorption effects were observed successfully when using these high-density CNT films.

In addition, many spherical core catalysts for CNT growth applications have been reported to date. For example, He *et al.* reported diameter- and length-dependent self-organization of CNTs on micro-spherical alumina particles with sizes of 3–10 μm .⁷ Park *et al.* prepared sea urchin-like CNT conjugates using a combination of spray pyrolysis and thermal CVD in the gas phase.⁸ Piao *et al.* prepared sea urchin-shaped CNTs using hollow carbon spheres that contained iron oxide on their surfaces.⁹ Kim *et al.* reported a semi-continuous fluidized-bed process that yielded CNT using approximately 500 μm -sized alumina beads as cores.¹⁰ Jo *et al.* investigated continuous-flow synthesis of carbon-coated silicon/iron silicide particles.¹¹ In addition, Boi *et al.* developed radial ferromagnetically filled-CNT structures.¹² Chen *et al.* reported sea urchin-like CNT/polyhedra structures starting from a zeolitic imidazolate framework (ZIF).¹³ Boron nitrate was also used as a core material to yield CNT conjugates.¹⁴ However, it is still difficult to accomplish homogeneous growth of dense CNTs with a uniform length from sub-micron-sized spherical core catalysts, because (i) core spherical catalysts larger than 1 μm in size are commercially available, but their sub-micron-sized counterparts are not easy to obtain; (ii) the availability of practical preparation techniques that can yield a variety of porous metal oxide cores with almost perfect spherical morphologies and sub-micron sizes is also limited; and (iii) the uniformity of the catalyst films on the catalyst supports is a specific feature of the magnetron sputtering method for planar substrates.

As an alternative, we have studied a unique and simple synthesis method to obtain sub-micron-sized spherical porous assemblies consisting of metal oxide nanoparticles using one-pot and single-step solvothermal reactions.¹⁵ For example, MgO,¹⁶ TiO₂,¹⁷ ZrO₂,^{18,19} Nb₂O₅,²⁰ SnO₂,²¹ and CeO₂ (ref. 22) assemblies were prepared successfully using this process. The assemblies obtained have almost perfect spherical morphologies with huge specific surface areas. We called these structures meso-/micro-porously architected roundly integrated metal oxide (MARIMO) particles.¹⁵ Composite MARIMOs, including several metal oxides, were synthesized easily using the solvothermal method, including Al₂O₃/TiO₂,²³ SiO₂/TiO₂,²⁴

Nb₂O₅/TiO₂,²⁵ SiO₂/ZrO₂,²⁶ ZrO₂/CeO₂,²⁷ PO_x/SnO₂,²¹ and CoO_x/MnO_y particles.²⁸ Industrial scale synthesis of some of these materials is also possible.²⁹ The MARIMOs obtained have characteristic nano-concave-convex surface structures and large numbers of pores that can capture noble metal nanoparticles effectively, leading them to support nanometal catalysts. Nanometal catalysts supported on MARIMOs such as Au/MARIMO TiO₂ for use in CO oxidation³⁰ and Ni/MARIMO ZrO₂ for dry reforming of methane^{19,26} were easy to prepare and exhibited high performance and durability when used in these reactions. Therefore, we speculated that our sub-micron-sized spherical catalysts would yield well-defined sea urchin-like CNT conjugates with uniform growth of CNTs if we used them as catalysts for CNT growth.

In this paper, preparation of spherical core catalysts suitable for CNT growth using the solvothermal method, detailed reaction conditions for production of CNT-MARIMO conjugates, and characterization of the conjugates obtained are discussed.

Experimental details

Materials

85% zirconium(IV) butoxide (Zr(O^{*n*}Bu)₄) in 1-butanol, iron(III) nitrate nonahydrate (Fe(NO₃)₃·9H₂O), cobalt(II) nitrate hexahydrate (Co(NO₃)₂·6H₂O), nickel(II) nitrate hexahydrate (Ni(NO₃)₂·6H₂O), zirconium dioxide (ZrO₂), cerium(III) nitrate hexahydrate (Ce(NO₃)₃·6H₂O), benzoic acid, diethylene glycol, acetonitrile, and methanol were purchased from FUJIFILM Wako Pure Chemical Corporation. Acetylacetone was obtained from Tokyo Chemical Industry Co., Ltd. Ethanol was purchased from Kishida Chemical Co., Ltd. UEP-100 ZrO₂ nanoparticles were obtained from Daiichi Kigenso Kagaku Kogyo Co., Ltd. All reagents were used as-received. TiO₂,^{15,17} ZrO₂,¹⁹ SnO₂,²¹ and CeO₂ (ref. 22) MARIMOs were prepared according to the previously reported procedure.

Synthesis of catalysts for CNT formation

Solvothermal method. Nanosized FeO_x catalysts embedded into porous Zr-based MARIMO support were solvothermally synthesized. First, Fe(NO₃)₃·9H₂O (13.7 mg, 0.0339 mmol) was dissolved in 0.70 mL of ethanol. 85% Zr(O^{*n*}Bu)₄ in 1-butanol (58.5 μL , 0.136 mmol) and acetylacetone (0.99 mL, 9.6 mmol) was then dissolved in 1.7 mL of ethanol, to which the Fe(NO₃)₃ solution in ethanol was added. The precursor solution obtained was stirred and then transferred to an SUS316 stainless steel pressure vessel with an inner volume of 10 mL; the vessel was then heated up to 250 °C and this temperature was maintained for 1 h. The reactor was then placed in an ice-water bath to quench the reaction. After it was cooled, the reaction mixture was washed several times with methanol using centrifugation and decantation. The powdery product obtained was then dried in a vacuum to yield 20 mg of s20-FeO_x/ZrO₂-M porous spheres; here, “s” and “M” denote “prepared by the solvothermal method” and “MARIMO support,” respectively, and the number following “s” represents the atomic percentage of the catalyst metal element (Fe) from the total amount of the catalyst



element (Fe) and the support metal element (Zr) (Table 1). Similar procedures using different amounts of $\text{Fe}(\text{NO}_3)_3 \cdot 9\text{H}_2\text{O}$ afforded fabrication of s5- $\text{FeO}_x/\text{ZrO}_2$ -M, s10- $\text{FeO}_x/\text{ZrO}_2$ -M, s30- $\text{FeO}_x/\text{ZrO}_2$ -M, and s50- $\text{FeO}_x/\text{ZrO}_2$ -M porous spheres. Similarly, s20- $\text{CoO}_x/\text{ZrO}_2$ -M and s20- $\text{NiO}_x/\text{ZrO}_2$ -M spheres were prepared using $\text{Co}(\text{NO}_3)_2 \cdot 6\text{H}_2\text{O}$ and $\text{Ni}(\text{NO}_3)_2 \cdot 6\text{H}_2\text{O}$, respectively. In addition, s20- $\text{NiO}_x/\text{ZrO}_2$ -M, s30- $\text{NiO}_x/\text{ZrO}_2$ -M, s50- $\text{NiO}_x/\text{ZrO}_2$ -M, and s70- $\text{NiO}_x/\text{ZrO}_2$ -M spheres were all prepared using $\text{Ni}(\text{NO}_3)_2 \cdot 6\text{H}_2\text{O}$ and $\text{Zr}(\text{O}^n\text{Bu})_4$ in 1-butanol as metal sources and diethylene glycol as an additive in acetonitrile. A similar solvothermal procedure using $\text{Fe}(\text{NO}_3)_3 \cdot 9\text{H}_2\text{O}$ and $\text{Ce}(\text{NO}_3)_3 \cdot 6\text{H}_2\text{O}$ as the metal sources and diethylene glycol and benzoic acid as additives in methanol yielded s50- $\text{FeO}_x/\text{CeO}_2$ -M spheres.

Impregnation method. The as-prepared ZrO_2 MARIMO support¹⁹ was calcined in air at 350 °C for 1 h. After cooling, 200 mg of the support was dispersed in 2.5 mL of reverse osmosis water. The resulting dispersion was then sonicated for several minutes. A solution of $\text{Fe}(\text{NO}_3)_3 \cdot 9\text{H}_2\text{O}$ (164 mg, 0.406 mmol) in 2.5 mL of reverse osmosis water was subsequently added to the dispersion. The resulting dispersion was mixed using a planetary centrifugal mixer (AR-100, Thinky) to produce a dry powder. This powder was then dried further at 110 °C for 2 h in an oven and subsequently calcined at 300 °C in air for 2 h to yield i20- $\text{FeO}_x/\text{ZrO}_2$ -M spheres, where “i” and “M” represent “prepared by the impregnation method” and “MARIMO support,” respectively; additionally, the number represents the atomic percentage of the catalyst metal element (Fe) from the total amount of the catalyst element (Fe) and the support metal element (Zr) (Table 2). A similar procedure with different quantities of $\text{Fe}(\text{NO}_3)_3 \cdot 9\text{H}_2\text{O}$ produced i5- $\text{FeO}_x/\text{ZrO}_2$ -M, i10- $\text{FeO}_x/\text{ZrO}_2$ -M, i30- $\text{FeO}_x/\text{ZrO}_2$ -M, and i50- $\text{FeO}_x/\text{ZrO}_2$ -M porous spheres. In a similar manner, a nanosized NiO_x catalyst impregnated in ZrO_2 MARIMO (i8- $\text{NiO}_x/\text{ZrO}_2$ -M) was prepared using $\text{Ni}(\text{NO}_3)_2 \cdot 6\text{H}_2\text{O}$. Nanosized FeO_x catalysts impregnated in commercially available ZrO_2 nanoparticles, denoted by i20- $\text{FeO}_x/\text{ZrO}_2$ -W and i20- $\text{FeO}_x/\text{ZrO}_2$ -U, were also prepared by the impregnation method, where “W” and “U” represent “Wako ZrO_2 ” and “UEP-100 ZrO_2 ,” respectively. Nanosized FeO_x was

Table 2 Catalysts prepared by the impregnation method

Sample name ^a	Catalyst metal oxide	Atomic ratio of catalyst metal/support metal in precursor solution
i8- $\text{NiO}_x/\text{ZrO}_2$ -M	NiO_x	7.6/92.4
i5- $\text{FeO}_x/\text{ZrO}_2$ -M	FeO_x	5/95
i10- $\text{FeO}_x/\text{ZrO}_2$ -M	FeO_x	10/90
i20- $\text{FeO}_x/\text{ZrO}_2$ -M	FeO_x	20/80
i30- $\text{FeO}_x/\text{ZrO}_2$ -M	FeO_x	30/80
i50- $\text{FeO}_x/\text{ZrO}_2$ -M	FeO_x	50/80
i20- $\text{FeO}_x/\text{ZrO}_2$ -W	FeO_x	20/80
i20- $\text{FeO}_x/\text{ZrO}_2$ -U	FeO_x	20/80
i20- $\text{FeO}_x/\text{TiO}_2$ -M	FeO_x	20/80
i20- $\text{FeO}_x/\text{SnO}_2$ -M	FeO_x	20/80
i20- $\text{FeO}_x/\text{CeO}_2$ -M	FeO_x	20/80

^a i, the number, M, W, and U represent prepared by the impregnation method, the atomic percentage of the catalyst metal element from the total amount of catalyst and support metal elements, MARIMO ZrO_2 , Wako ZrO_2 and UEP-100 ZrO_2 , respectively.

also impregnated in MARIMO TiO_2 , MARIMO SnO_2 , and MARIMO CeO_2 to yield i20- $\text{FeO}_x/\text{TiO}_2$ -M, i20- $\text{FeO}_x/\text{SnO}_2$ -M, and i20- $\text{FeO}_x/\text{CeO}_2$ -M spheres, respectively.

Characterization. Transmission electron microscopy (TEM) and scanning electron microscopy (SEM) images of the catalysts were acquired using a JEOL JEM-2100F microscope and a Hitachi SU8020 microscope, respectively. Energy-dispersive X-ray spectroscopy (EDX) measurements were performed using an Oxford INCA X-Max 80 EDX spectrometer attached to the TEM and a HORIBA X-Max80 spectrometer attached to the SEM. X-ray diffraction (XRD) patterns were recorded using both Rigaku SmartLab and Rigaku SmartLab SE diffractometers with nickel-filtered $\text{Cu-K}\alpha$ radiation (X-ray wavelength: 1.5418 Å). Nitrogen adsorption/desorption isotherms were obtained using the MicrotracBEL BELSORP-mini X and BELSORP-mini II instruments at 77 K. Specific surface areas were calculated *via* the Brunauer–Emmett–Teller (BET) method. Pore size distribution

Table 1 Catalysts prepared by the solvothermal method

Sample name ^a	Catalyst metal oxide	Atomic ratio of catalyst metal/support metal in precursor solution	Metal sources	Additive	Solvent
s5- $\text{FeO}_x/\text{ZrO}_2$ -M	FeO_x	5/95	$\text{Fe}(\text{NO}_3)_3 + \text{Zr}(\text{O}^n\text{Bu})_4$	Acetylacetone	Ethanol
s10- $\text{FeO}_x/\text{ZrO}_2$ -M	FeO_x	10/90	$\text{Fe}(\text{NO}_3)_3 + \text{Zr}(\text{O}^n\text{Bu})_4$	Acetylacetone	Ethanol
s20- $\text{FeO}_x/\text{ZrO}_2$ -M	FeO_x	20/80	$\text{Fe}(\text{NO}_3)_3 + \text{Zr}(\text{O}^n\text{Bu})_4$	Acetylacetone	Ethanol
s30- $\text{FeO}_x/\text{ZrO}_2$ -M	FeO_x	30/70	$\text{Fe}(\text{NO}_3)_3 + \text{Zr}(\text{O}^n\text{Bu})_4$	Acetylacetone	Ethanol
s50- $\text{FeO}_x/\text{ZrO}_2$ -M	FeO_x	50/50	$\text{Fe}(\text{NO}_3)_3 + \text{Zr}(\text{O}^n\text{Bu})_4$	Acetylacetone	Ethanol
s20- $\text{CoO}_x/\text{ZrO}_2$ -M	CoO_x	20/80	$\text{Co}(\text{NO}_3)_2 + \text{Zr}(\text{O}^n\text{Bu})_4$	Acetylacetone	Ethanol
s20- $\text{NiO}_x/\text{ZrO}_2$ -M	NiO_x	20/80	$\text{Ni}(\text{NO}_3)_2 + \text{Zr}(\text{O}^n\text{Bu})_4$	Acetylacetone	Ethanol
s30- $\text{NiO}_x/\text{ZrO}_2$ -M	NiO_x	30/70	$\text{Ni}(\text{NO}_3)_2 + \text{Zr}(\text{O}^n\text{Bu})_4$	Diethylene glycol	Acetonitrile
s50- $\text{NiO}_x/\text{ZrO}_2$ -M	NiO_x	50/50	$\text{Ni}(\text{NO}_3)_2 + \text{Zr}(\text{O}^n\text{Bu})_4$	Diethylene glycol	Acetonitrile
s70- $\text{NiO}_x/\text{ZrO}_2$ -M	NiO_x	70/30	$\text{Ni}(\text{NO}_3)_2 + \text{Zr}(\text{O}^n\text{Bu})_4$	Diethylene glycol	Acetonitrile
s50- $\text{FeO}_x/\text{CeO}_2$ -M	FeO_x	50/50	$\text{Fe}(\text{NO}_3)_3 + \text{Ce}(\text{NO}_3)_3$	Diethylene glycol + benzoic acid	Methanol

^a s, the number, and M represent prepared by the solvothermal method, the atomic percentage of the catalyst metal element from the total amount of catalyst and support metal elements and MARIMO ZrO_2 , respectively.



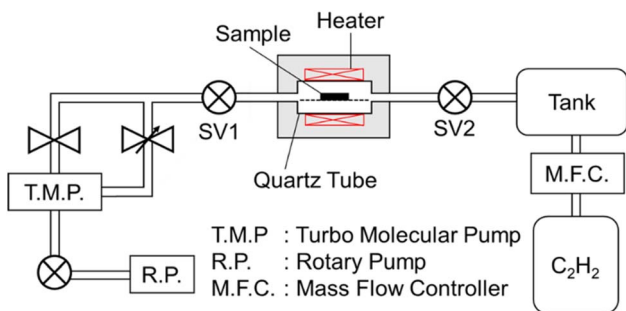


Fig. 1 Schematic illustration of the thermal chemical vapor deposition apparatus.

was estimated by the Barrett–Joyner–Halenda (BJH) method. Raman spectra were observed to evaluate the crystallinity of the CNTs on a Horiba HR-800 Raman spectrometer under excitation at a laser wavelength of 532 nm.

Thermal chemical vapor deposition. The CVD instrument was set up as described in previous reports.^{5,6} A schematic illustration of the setup is shown in Fig. 1. An aliquot amount of the MARIMO catalyst was dispersed in either methanol or acetone. The dispersion was then drop-cast on a thermal CVD SiO₂ (th-SiO₂) substrate. The thickness of the oxide layer of th-SiO₂ substrates, formed by thermal CVD on Si substrates, was 100 nm. After drying, the th-SiO₂ substrate with the catalyst was transferred into the quartz tube of the CVD instrument. The catalysts on the th-SiO₂ substrate in the quartz tube were dried at 120 °C under vacuum conditions until the pressure reached less than 5.0×10^{-4} Pa. The reactor temperature was raised to 730 °C. Ethyne (C₂H₂) gas was then introduced into the tube with a 10 sccm gas flow under pressure of 65 Pa for 10 s, and the reactor was then cooled to room temperature.

Results and discussion

Synthesis of the core MARIMO catalysts

Nanosized metal oxide catalysts supported in the MARIMO sub-micron-sized spheres were synthesized by two different methods: the one-pot solvothermal method and the two-step impregnation method. Fig. 2 illustrates the two synthesis

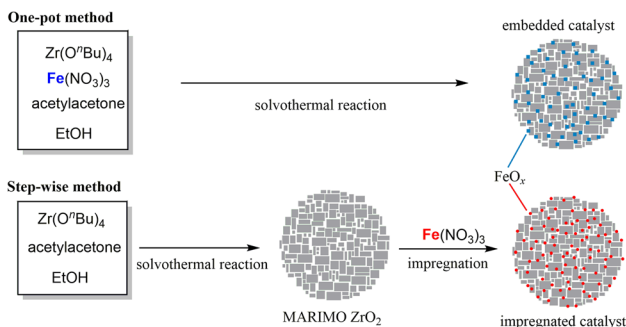


Fig. 2 One-pot solvothermal synthesis of FeO_x catalyst embedded in ZrO₂ MARIMO (top) and step-wise preparation of FeO_x catalyst impregnated in MARIMO ZrO₂ (bottom).

approaches used to yield FeO_x catalysts supported in/on MARIMO ZrO₂ as an example.

First, nanosized metal oxide catalysts (FeO_x, CoO_x, and NiO_x) that was embedded in the support metal oxides were prepared using our original one-pot and single-step solvothermal method.¹⁹ The synthesis procedure was very simple. For example, a precursor solution that included Zr(OⁿBu)₄, Fe(NO₃)₃·9H₂O, and acetylacetone in ethanol was heated up to 250 °C in an SUS316 pressure vessel. The powdery product obtained was washed with methanol and dried in a vacuum, yielding sFeO_x/ZrO₂-M with different FeO_x contents (see Table 1). In the sNiO_x/ZrO₂-M case except for s20-NiO_x/ZrO₂-M, a solution that included Zr(OⁿBu)₄, Ni(NO₃)₂·6H₂O, and diethylene glycol in acetonitrile was used as the precursor solution. The combination of Co(NO₃)₂ and Zr(OⁿBu)₄ with acetylacetone in ethanol and the combination of Fe(NO₃)₃ and Ce(NO₃)₃ with diethylene glycol and benzoic acid in methanol produced sCoO_x/ZrO₂-M and sFeO_x/CeO₂-M spheres, respectively, using procedures that were slightly modified relative to the previously reported method.^{19,22}

Nanosized metal oxide catalysts (FeO_x, CoO_x, and NiO_x) that were impregnated in the support metal oxides (TiO₂, ZrO₂, SnO₂, and CeO₂) were prepared by the conventional impregnation method, which is quite a versatile technique in the catalyst preparation field for fabrication of supported nanometal catalysts.³¹ TiO₂,¹⁵ ZrO₂,¹⁹ SnO₂,²¹ and CeO₂ (ref. 22) MARIMOs were prepared using the previously reported solvothermal methods; these oxides are ideal materials for dispersion of catalyst metal (oxide) particles on their surfaces because they have unique nano-concave-convex surfaces, high specific surface areas (150–220 m² g^{−1}; see Fig. S1 and Table S1†), and large numbers of pores for good dispersion of the nanometal oxide catalysts used for CNT growth. FeO_x was loaded on these MARIMOs by the impregnation method using Fe(NO₃)₃·9H₂O to yield i5-FeO_x/ZrO₂-M, i10-FeO_x/ZrO₂-M, i20-FeO_x/ZrO₂-M, i30-FeO_x/ZrO₂-M, i50-FeO_x/ZrO₂-M, i20-FeO_x/TiO₂-M, i20-FeO_x/SnO₂-M, and i20-FeO_x/CeO₂-M spheres (Table 2). Similarly, i20-FeO_x/ZrO₂-W and i20-FeO_x/ZrO₂-U spheres were also prepared as reference catalysts by the impregnation method, where “W” and “U” represent “Wako ZrO₂” and “UEP-100 ZrO₂,” respectively. Similarly, NiO_x was loaded on ZrO₂-M using Ni(NO₃)₂·6H₂O to yield i8-NiO_x/ZrO₂-M.

Physical properties of the core MARIMO catalysts

Specific surface areas of impregnated catalysts. We have studied the solvothermal synthesis of spherical porous aggregates of metal oxide(s) called MARIMO particles. The main characteristic of the process is the simple one-pot, single-step reaction that yields embedded nanosized catalysts in porous metal oxide supports with spherical morphologies, high porosity, and nano-convex-concave surface structures. We applied this technique to produce FeO_x, CoO_x, and NiO_x catalysts embedded in MARIMO ZrO₂ support.

Specific surface areas of the solvothermally embedded catalysts were estimated to compare with those of native MARIMO supports. In the cases of sFeO_x/ZrO₂-M, s20-CoO_x/ZrO₂-M, and



s20-NiO_x/ZrO₂-M, their specific surface areas are so high (182–269 m² g⁻¹) (see Fig. S1 and Table S1†). However, further incorporation of NiO_x into ZrO₂-M support by the solvothermal method resulted in drastic decrease of the specific surface areas (6–36 m² g⁻¹), which can be ascribed to blockage of the pores of the MARIMO supports with the much amount of the introduced nanosized catalyst metal oxides as BJH plots indicate (see Fig. S1B†). Similarly, s50-FeO_x/CeO₂-M also exhibited quite low specific surface area (8 m² g⁻¹).

Microscope observations and XRD spectra. SEM images of the catalysts obtained from the procedures above are shown in Fig. 3 and 4. Scanning TEM (STEM)-EDX and SEM-EDX images of the catalysts obtained for elemental analysis are shown in Fig. S2 and S3.† Atomic ratios obtained from the elemental analysis on STEM/EDX or SEM/EDX are listed in Tables S2 and S3.† The XRD spectra are shown in Fig. S4 and S5.†

As shown in Fig. 3A–C, ZrO₂ catalysts that included 5 to 20 atom% FeO_x with striking spherical morphologies were obtained; their XRD spectra showed quite broad peaks that were ascribed to cubic ZrO₂ (see Fig. S4A–C†). Judging from the peak positions (2θ), FeO_x, CoO_x, or NiO_x did not yield solid solutions with MARIMO ZrO₂ support (see Fig. S4†). Further introduction of larger amounts of FeO_x caused swellings on the MARIMO surfaces (Fig. 3D and E), for which the corresponding XRD spectra showed clear peaks that were ascribed to cubic Fe₃O₄ (see Fig. S3D and E†). Therefore, introduction of too much FeO_x caused irregular shapes to occur and led to the formation of large-sized Fe₃O₄ particles. In contrast, 20 atom% CoO_x catalyst embedded in ZrO₂ MARIMO produced perfectly spherical

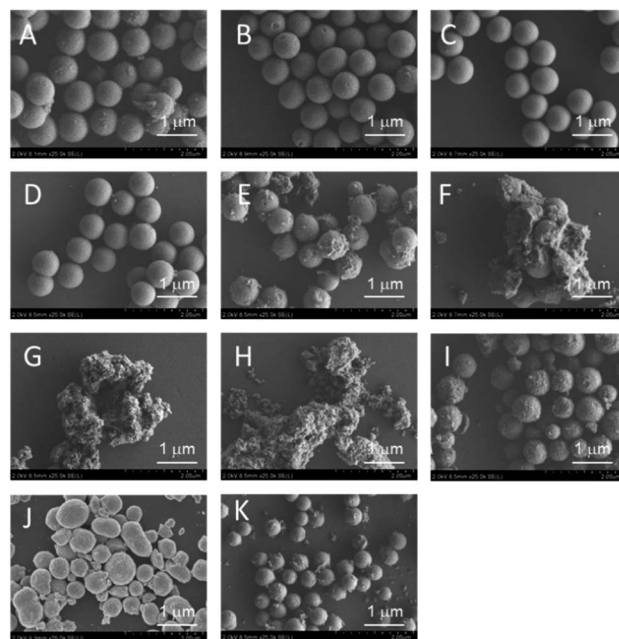


Fig. 4 SEM images of catalysts prepared using the impregnation method. (A) i8-NiO_x/ZrO₂-M, (B) i5-FeO_x/ZrO₂-M, (C) i10-FeO_x/ZrO₂-M, (D) i20-FeO_x/ZrO₂-M, (E) i30-FeO_x/ZrO₂-M, (F) i50-FeO_x/ZrO₂-M, (G) i20-FeO_x/ZrO₂-W, (H) i20-FeO_x/ZrO₂-U, (I) i20-FeO_x/TiO₂-M, (J) i20-FeO_x/SnO₂-M and (K) i20-FeO_x/CeO₂-M.

morphologies (Fig. 3F). In addition, 20–70 atom% NiO_x catalysts embedded in ZrO₂ MARIMOs also exhibited perfectly spherical morphologies (Fig. 3G–J). 50 atom% FeO_x catalyst embedded in CeO₂ MARIMO also showed a spherical morphology, including both large- and small-sized spheres (Fig. 3K).

As an alternative, the impregnation method is a simple preparation technique that can be used to obtain supported catalysts.³¹ In addition, this method is a versatile technique that is applicable to almost all types of support. We applied this technique to obtain NiO_x and FeO_x catalysts that were supported on several types of MARIMO support. XRD spectra indicated that the ZrO₂ MARIMO supports for the impregnated catalysts showed a cubic crystal phase (see Fig. S5B–F†). Interestingly, i8-NiO_x/ZrO₂-M consisted of cubic and monoclinic crystal phases (see Fig. S5A†). The inherently spherical morphologies of the MARIMO supports were clearly preserved in the cases of 5 to 20 atom% impregnation of NiO_x and FeO_x in the ZrO₂ MARIMO (Fig. 4A–D). However, further loading of larger quantities of FeO_x into the ZrO₂ MARIMO (30 and 50 atom%) resulted in catalysts with rugged structures (Fig. 4E and F). Therefore, loading of more than 30 atom% of FeO_x on the ZrO₂ MARIMO support by the impregnation method was not suitable for our purpose of preparing spherical catalysts for CNT growth. Furthermore, commercially available ZrO₂ particles, comprising the Wako ZrO₂ and UEP-100 ZrO₂ particles, without spherical morphologies were also converted into FeO_x/ZrO₂ catalysts *via* the impregnation method to act as reference samples (Fig. 4G and H, respectively), with the ZrO₂ supports showing a monoclinic crystal phase in this case (see Fig. S5G

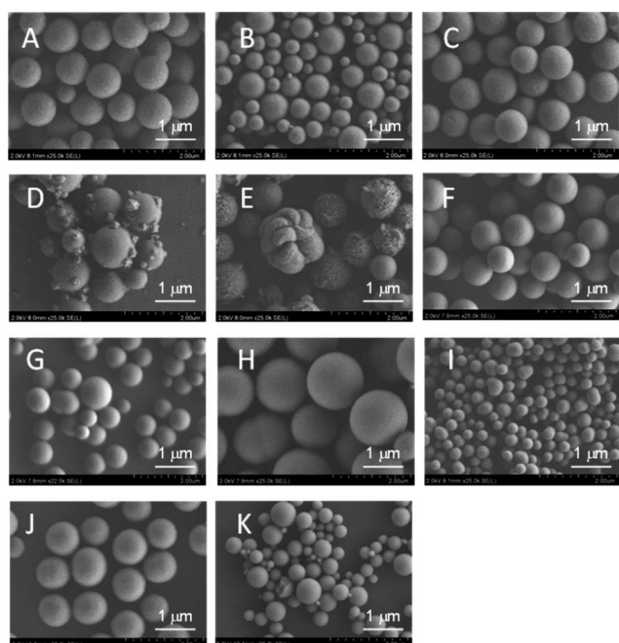


Fig. 3 SEM images of catalysts prepared using the solvothermal method. (A) s5-FeO_x/ZrO₂-M, (B) s10-FeO_x/ZrO₂-M, (C) s20-FeO_x/ZrO₂-M, (D) s30-FeO_x/ZrO₂-M, (E) s50-FeO_x/ZrO₂-M, (F) s20-CoO_x/ZrO₂-M, (G) s20-NiO_x/ZrO₂-M, (H) s30-NiO_x/ZrO₂-M, (I) s50-NiO_x/ZrO₂-M, (J) s70-NiO_x/ZrO₂-M and (K) s50-FeO_x/CeO₂-M.



and H^+). In the cases of the spherical TiO_2 , SnO_2 , and CeO_2 MARIMO supports, globular morphologies were observed for the impregnated catalysts after FeO_x loading (Fig. 4I–K, respectively). Therefore, we prepared catalyst candidate materials to obtain the MARIMO-CNT conjugates successfully.

Thermal CVD of the prepared catalysts

Embedded catalysts obtained by one-pot solvothermal synthesis. As a first test, thermal CVD using ethyne gas as a carbon source was performed under conditions of a temperature of 730 °C, pressure of 65 Pa, 10 sccm ethyne gas flow, and a reaction time of 10 s using 20 atom% FeO_x , CoO_x , and NiO_x catalysts that were solvothermally embedded in MARIMO ZrO_2 and CeO_2 supports. The performances of these catalysts were evaluated *via* SEM observations (Fig. 5). As a result, the FeO_x catalyst embedded in MARIMO ZrO_2 showed the best results, producing CNT-hair (Fig. 5A) rather than CNT sea urchin structures, as compared with the other CoO_x (Fig. 5B) and NiO_x (Fig. 5C) catalysts embedded in MARIMO ZrO_2 . In addition, the combination of FeO_x/CeO_2 resulted in poor growth of CNTs with low density (Fig. 5D). Therefore, the CNT-hair growth process is strongly dependent on the combination of the nanosized metal oxide catalyst and the support metal oxide. In our case, the combination of the nanosized FeO_x catalyst with ZrO_2 as the support (FeO_x/ZrO_2) produced the best results for formation of the CNT-hair.

Next, the amount of loaded Fe was varied to optimize the CNT-hair formation process (Fig. 6). The amount and the length of CNT-hair increased for Fe loading of up to 20 atom% (Fig. 6A–C), but the spherical catalyst cores themselves can be seen through the CNT-hair when the amount of Fe exceeded 30 atom% (Fig. 6D and E). Therefore, we decided to use 20 atom% of Fe catalyst in the later experiments.

The reaction temperature was varied (670, 730, and 760 °C) while using $s20-FeO_x/ZrO_2-M$ as the catalyst (Fig. 7). The CNT-hair seemed to grow well at all temperatures tested. To determine the quality of the CNTs, the I_G/I_D intensity ratios in the Raman spectra were estimated (see Fig. S6†), whose ratios of the G and D bands (I_G/I_D) in the Raman spectra were used to determine the crystallinity of the CNT-hair obtained. G band, in-

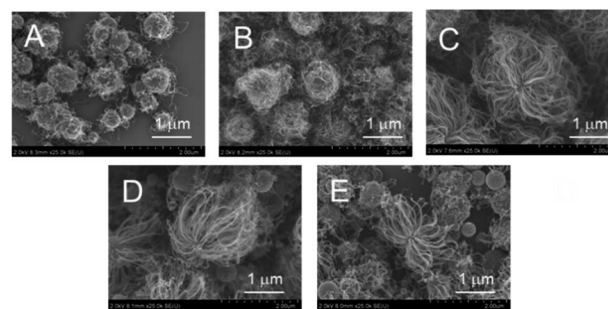


Fig. 6 SEM images of CNT-hair obtained using different quantities of catalysts, including (A) $s5-FeO_x/ZrO_2-M$, (B) $s10-FeO_x/ZrO_2-M$, (C) $s20-FeO_x/ZrO_2-M$ (the same as Fig. 5A), (D) $s30-FeO_x/ZrO_2-M$ and (E) $s50-FeO_x/ZrO_2-M$ at 730 °C under pressure of 65 Pa with a 10 sccm ethyne gas flow for 10 s.

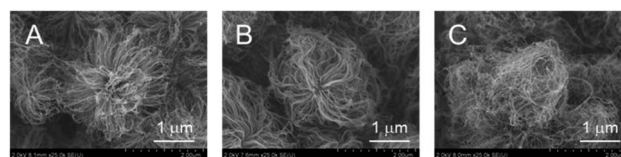


Fig. 7 SEM images of CNT-hair obtained using $s20-FeO_x/ZrO_2-M$ catalysts at temperatures of (A) 670 °C, (B) 730 °C (the same as Fig. 5A) and (C) 760 °C under pressure of 65 Pa with a 10 sccm ethyne gas flow for 10 s.

plane bond stretching mode of the C–C bonds in the hexagonal lattice,³² represents the higher concentration of sp^2 carbon atoms and higher-ordered graphitic structures. While the D band, hexagonal sp^2 breathing mode, indicates the presence of defects in sp^2 network.³³ The CNT-hair obtained at 730 °C (1.88) was found to show the best crystallinity than those obtained at 670 °C (0.71) and 760 °C (0.82).

With regard to the reaction time, small perturbances were observed with the short reaction time of 0.5 s (Fig. 8A), while CNT-hair of sufficient length was produced after 10 s (Fig. 8D), this indicating that a sufficient quantity of the ethyne gas is indispensable for formation of the CNT-hair conjugates.

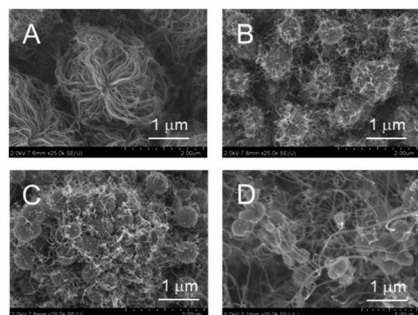


Fig. 5 SEM images of CNT-hair obtained using different catalysts, including (A) $s20-FeO_x/ZrO_2-M$, (B) $s20-CoO_x/ZrO_2-M$, (C) $s20-NiO_x/ZrO_2-M$ and (D) $s50-FeO_x/CeO_2-M$ at 730 °C under pressure of 65 Pa with a 10 sccm ethyne gas flow for 10 s.

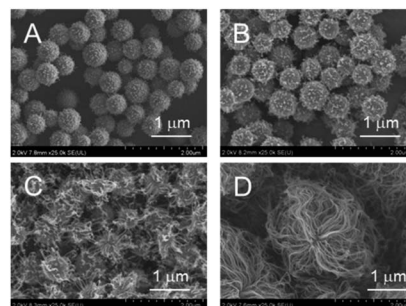


Fig. 8 SEM images of products obtained using $s20-FeO_x/ZrO_2-M$ catalysts with different reaction times at 730 °C under pressure of 65 Pa with a 10 sccm ethyne gas flow. (A) 0.5 s, (B) 1 s, (C) 3 s and (D) 10 s (the same as Fig. 5A).



In summary for this section, in which nanosized metal oxide catalysts embedded in metal oxide supports were used, the reaction conditions when using the s20-FeO_x/ZrO₂-M catalysts at 730 °C under pressure of 65 Pa with 10 sccm ethyne gas flow for 10 s were the best conditions for CNT-hair formation.

Impregnated catalysts obtained by two-step impregnation method. Catalysts obtained by the impregnation method were also subjected to thermal CVD. With regard to the catalyst supports, nanosized FeO_x catalysts impregnated in TiO₂ and SnO₂ MARIMOs did not yield CNTs (Fig. 9A and C), while those impregnated in ZrO₂ and CeO₂ MARIMOs yielded CNT-hair effectively (Fig. 9B and D). Of the two supports, ZrO₂ seemed to be a better support than CeO₂ based on the amount of CNT-hair obtained. As a matter of course, the reference nanosized FeO_x catalysts impregnated into the commercially available ZrO₂ nanoparticles without spherical morphologies did not produce CNT-hair (Fig. 9E and F).

The quantities of the loaded FeO_x were critical to effective production of the CNT-hair. Smaller amounts of Fe atoms (5 and 10 atom%) in the MARIMO ZrO₂ support were not effective in yielding CNT-hair (Fig. 10A and B). However, larger quantities of Fe atoms (20 atom%) on the MARIMO ZrO₂ support led to effective CNT-hair growth (Fig. 10C). The reaction temperature was also important to the formation of the CNT-hair. Almost zero CNT-hair formation was observed at the lower temperature of 670 °C (Fig. 11A). However, use of the higher temperatures of 730 °C and 760 °C resulted in the formation of satisfactory CNT-hair (Fig. 11B and C).

As a conclusion for thermal CVD of the prepared catalysts Section, the combination of nanosized FeO_x as the CNT

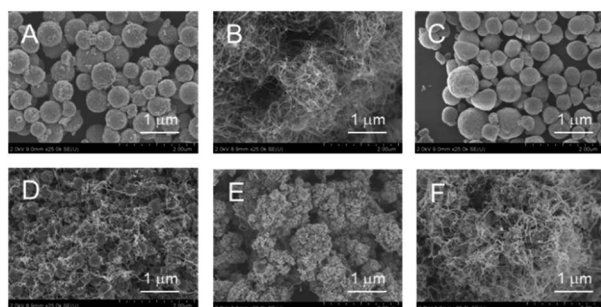


Fig. 9 SEM images of products obtained using FeO_x catalysts supported on different metal oxides. (A) i20-FeO_x/TiO₂-M, (B) i20-FeO_x/ZrO₂-M, (C) i20-FeO_x/SnO₂-M, (D) i20-FeO_x/CeO₂-M, (E) i20-FeO_x/ZrO₂-W and (F) i20-FeO_x/ZrO₂-U at 730 °C under pressure of 65 Pa with a 10 sccm ethyne gas flow for 10 s.

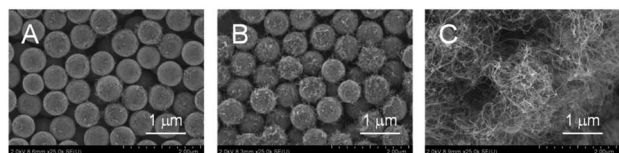


Fig. 10 SEM images of products obtained using catalysts with different quantities of FeO_x. (A) i5-FeO_x/ZrO₂-M, (B) i10-FeO_x/ZrO₂-M and (C) i20-FeO_x/ZrO₂-M (the same as Fig. 9B) at 730 °C under pressure of 65 Pa with a 10 sccm ethyne gas flow for 10 s.

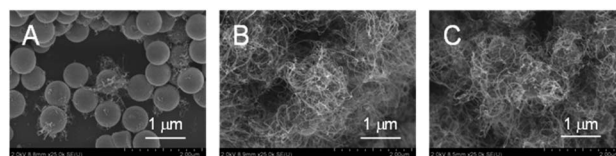


Fig. 11 SEM images of products obtained using i20-FeO_x/ZrO₂-M at different temperatures. (A) 670 °C, (B) 730 °C (the same as Fig. 9B) and (C) 760 °C under pressure of 65 Pa with a 10 sccm ethyne gas flow for 10 s.

catalyst and ZrO₂ as the support was shown to be the best for production of CNT-hair under our reaction conditions, irrespective of use of a solvothermally embedded or impregnated FeO_x/ZrO₂ catalyst. In light of all the results obtained, we concluded that the best catalyst for CNT-hair formation was the 20 atom% FeO_x catalyst supported in the MARIMO ZrO₂ porous spheres. From this point, the reaction conditions were fixed as follows: use of the 20 atom% FeO_x/ZrO₂ catalyst at 730 °C under pressure of 65 Pa with a 10 sccm ethyne gas flow for 10 s.

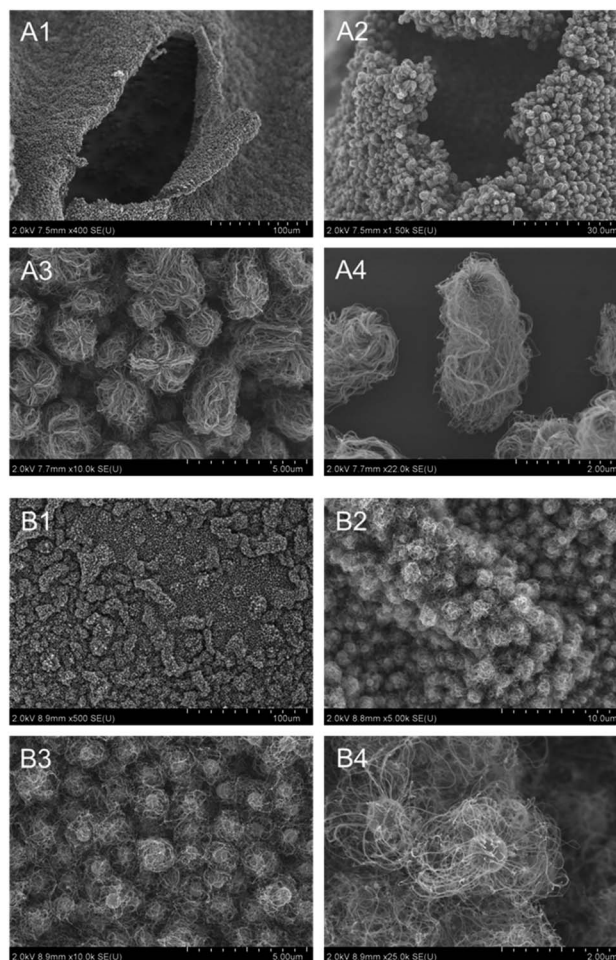


Fig. 12 SEM images of CNT-hairs at different magnifications obtained using (A) s20-FeO_x/ZrO₂-M and (B) i20-FeO_x/ZrO₂-M catalysts at 730 °C under pressure of 65 Pa with a 10 sccm ethyne gas flow for 10 s.



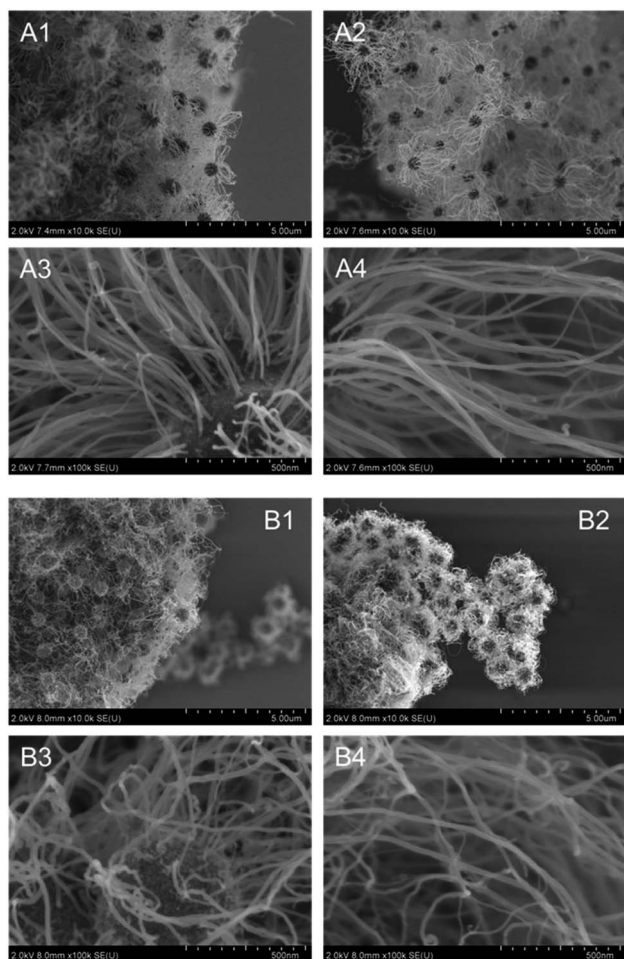


Fig. 13 SEM images of CNT-hairs at different magnifications obtained using (A) s20-FeO_x/ZrO₂-M and (B) i20-FeO_x/ZrO₂-M catalysts at 730 °C under pressure of 65 Pa with a 10 sccm ethyne gas flow for 10 s.

Detailed observation of the CNT-hair

Fig. 12 shows SEM images of the products obtained using the solvothermally embedded s20-FeO_x/ZrO₂-M catalyst (Fig. 12A) and the impregnated i20-FeO_x/ZrO₂-M catalyst (Fig. 12B). In the embedded s20-FeO_x/ZrO₂-M case, a waved sheet-like product on a th-SiO₂ substrate was observed under low magnification (Fig. 12A1). Expansion of the ripped area shows that the sheet consists of large numbers of particles (Fig. 12A2). The 5 μm-scale image clearly indicates that these particles are aggregates of multiple yarns, similar to fuzzy balls or cotton candies, with diameters of less than 3 μm (Fig. 12A3). Further expansion clearly shows that the aggregates include dark spherical cores and long gray threads (*ca.* 3 nm in length) (Fig. 12A4), which can be ascribed to the FeO_x/ZrO₂ MARIMO core and the CNTs, respectively. In the same manner, the impregnated i20-FeO_x/ZrO₂-M catalyst produced similar CNT-hair (Fig. 12B), but the density of the CNTs on the impregnated i20-FeO_x/ZrO₂-M catalyst appeared to be slightly lower than that obtained on the embedded s20-FeO_x/ZrO₂-M catalyst (Fig. 12A3, A4, B3, B4 and S7, S8†).

Further expansions clearly show that the CNTs grew upward from the surface of the core FeO_x/ZrO₂ MARIMOS (Fig. 13A3, A4, B3 and B4). Another unique feature of the CNT-hair can be seen in Fig. 13A1, A2, B1 and B2. The CNT-hairs were entangled with each other to show a structure similar to a nonwoven fabric, which constructs CNT grids with junctions formed by the ZrO₂ MARIMOS. Furthermore, the combination of the black core FeO_x/ZrO₂ MARIMOS with the CNTs appears similar to frog eggs. A single long CNT is soft and flexible. However, when multiple CNTs come together, they support each other, creating a new CNT forest morphology.^{5,6} Similar to the CNT forest, the CNTs in the CNT-hair are soft and flexible. However, when large numbers of CNT-hairs come together, they become tangled with each other, yielding a new morphology like the observed CNT-

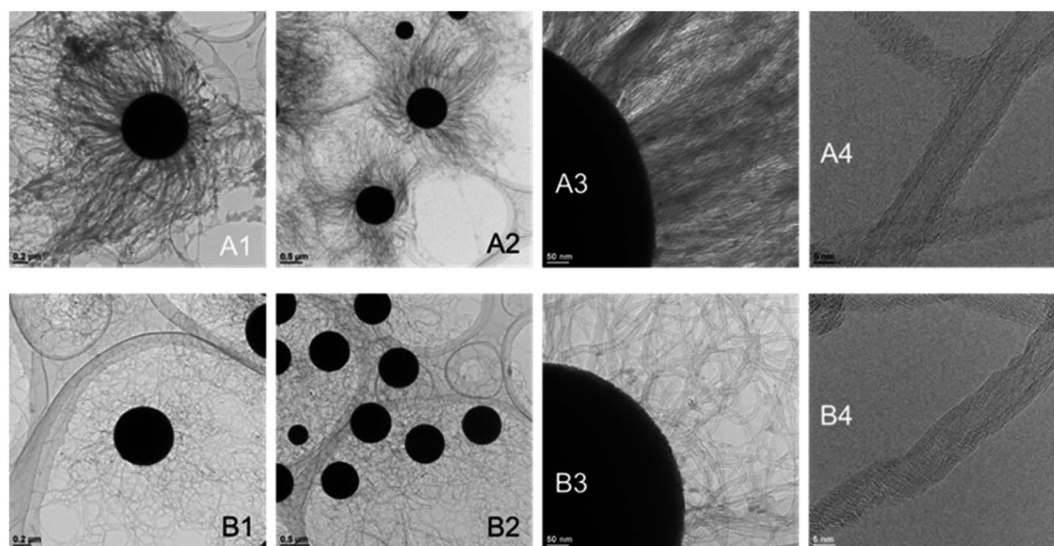


Fig. 14 TEM images of CNT-hairs at different magnifications obtained using (A) s20-FeO_x/ZrO₂-M and (B) i20-FeO_x/ZrO₂-M catalysts at 730 °C under pressure of 65 Pa with a 10 sccm ethyne gas flow for 10 s.



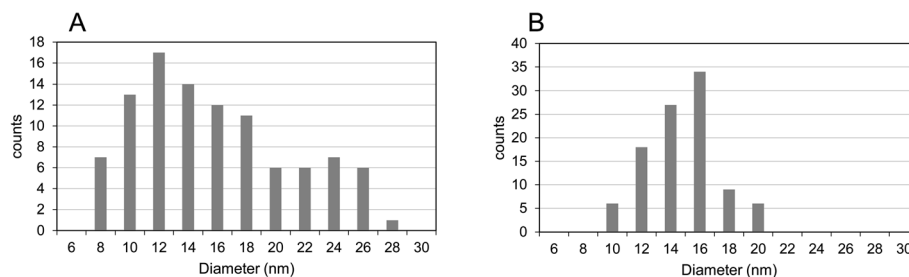


Fig. 15 Diameter distributions of CNT-hairs obtained using (A) s20-FeO_x/ZrO₂-M catalyst and (B) i20-FeO_x/ZrO₂-M catalyst at 730 °C under pressure of 65 Pa with a 10 sccm ethyne gas flow for 10 s.

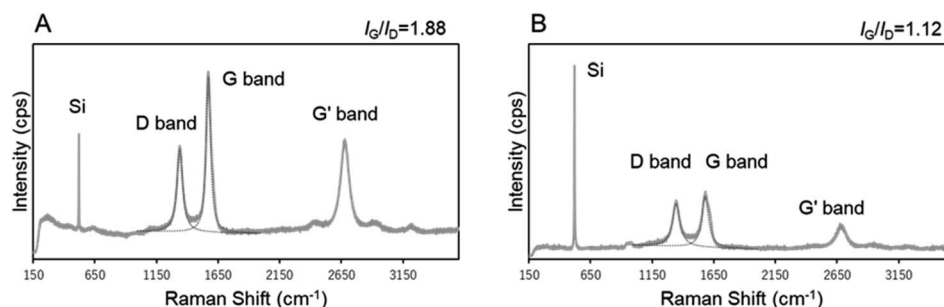


Fig. 16 Raman spectra of CNT-hairs obtained using (A) s20-FeO_x/ZrO₂-M and (B) i20-FeO_x/ZrO₂-M catalysts at 730 °C under pressure of 65 Pa with a 10 sccm ethyne gas flow for 10 s. The Si peaks at 520 cm⁻¹ were observed in both samples on the th-SiO₂ substrates on which MARIMO catalysts were drop-cast.

frog eggs structure. Based on these observations, the layered materials obtained by constructed with large amounts of CNT-hair can show intriguing physical properties, including isotropic absorption of polarized electromagnetic waves.

TEM images clearly show that the CNT-hairs grew from the surface of the core MARIMO catalysts regardless of whether the catalyst was embedded or impregnated (Fig. 14). In addition, the CNTs obtained were ascertained to be multi-walled structures with 5–8 layers. To determine the diameter distribution of the CNT-hairs, the diameters of 100 tubes in the TEM images were estimated (Fig. 15). As a result, the CNT diameter distribution obtained when using the embedded s20-FeO_x/ZrO₂-M catalyst showed two maxima of 12 and 24 nm, with an average value of 14.8 nm and a 5.4 nm dispersion, while the corresponding results obtained using the impregnated i20-FeO_x/ZrO₂-M catalyst showed a smaller average value (13.8 nm) with a lower dispersion (2.3 nm). Therefore, the CNT-hair obtained using the embedded s20-FeO_x/ZrO₂-M catalyst was dense, thick, and straight, while that obtained using the impregnated i20-FeO_x/ZrO₂-M catalyst was a little sparse, thin, and curly (see Fig. 12–15).

To determine the crystallinity of the CNT-hair obtained, the intensity ratios of the G and D bands I_G/I_D in the Raman spectra were estimated (Fig. 16). Consequently, the CNT-hair obtained using s20-FeO_x/ZrO₂-M (1.88) was found to show better crystallinity than that obtained using i20-FeO_x/ZrO₂-M (1.12). The G' (or 2D) band at around 2700 cm⁻¹ originates from the second-order Raman scattering, arising from a two-phonon, intervalley, second-order Raman scattering process.³⁴ The sharp and higher

intensity of the G' band represents the lower concentration of defects and disorders and lower interaction between graphene layers, indicating a high-quality lower number of layers, especially for single-walled carbon nanotubes. The intensity ratio of the G' and G band in CNTs grown at 730 °C on s20-FeO_x/ZrO₂-M ($I_{G'}/I_G = 0.56$) was higher than that on i20-FeO_x/ZrO₂-M catalysts ($I_{G'}/I_G = 0.45$). Sharp G' band and higher I_G/I_D of CNTs on s20-FeO_x/ZrO₂-M catalysts indicate higher quality of carbon nanotube formation, compared with i20-FeO_x/ZrO₂-M catalysts. As shown in Fig. 14A4 and B4, crystal structure order was confirmed higher for CNTs on s20-FeO_x/ZrO₂-M catalysts (Fig. 14A4) compared with i20-FeO_x/ZrO₂-M catalysts (Fig. 14B4).

Conclusions

Catalysts that were suitable for CNT-hair preparation were studied extensively. FeO_x, CoO_x, and NiO_x were selected as the CNT catalysts, and TiO₂, ZrO₂, SnO₂, and CeO₂ were selected as the support materials. Supported catalysts with different combinations of these catalysts and supports were prepared by two different methods, comprising the one-step solvothermal method and the two-step impregnation method, and yielded impregnated catalysts and embedded catalysts, respectively. Among the catalyst candidates, the combination of FeO_x as the catalyst for CNT growth and ZrO₂ as the support resulted in the best growth of CNTs under the required reaction conditions of a temperature of 730 °C under pressure of 65 Pa with a 10 sccm ethyne gas flow for a reaction time of 10 s. These CNTs consisted

of 5–8 layered multi-wall structures and the length of these CNTs reached approximately 3 μm . The CNT-hair that was obtained using the solvothermally embedded catalyst showed higher crystallinity and was dense, thick, and straight, while that obtained using the impregnated catalyst was a little sparse, thin, and curly. A unique structure consisting of multiple CNT yarns, similar to fuzzy balls or cotton candies, was produced. Multiple CNT-hair conjugates came together to yield a layer structure, in which the core $\text{FeO}_x/\text{ZrO}_2$ catalysts and CNT yarns appeared to be structured like frog eggs. Based on these observations, the layer materials obtained from construction with large amounts of CNT-hair are expected to exhibit intriguing physical properties, including isotropic absorption of polarized light and electromagnetic waves. Further studies of the physical properties of these materials are now in progress.

Author contributions

Kazuya Kobiro: funding acquisition, project administration, resources, supervision, writing – review & editing. Hinako Kimura: data curation, formal analysis, investigation, methodology, visualization. Saki Hirose: data curation, formal analysis, investigation, methodology, visualization. Makoto Kinjo: data curation, formal analysis, investigation. Hiroshi Furuta: conceptualization, methodology, project administration, writing – review & editing.

Conflicts of interest

There are no conflicts to declare.

Acknowledgements

This work was partially supported by the JSPS KAKENHI (grant numbers 20K05093 and 22K04819). We thank David MacDonald, MSc, from Edanz (<https://jp.edanz.com/ac>) for editing a draft of this manuscript.

References

- 1 S. Iijima, *Nature*, 1991, **354**, 56–57.
- 2 D. Y. Kim, H. Sugime, K. Hasegawa, T. Osawa and S. Noda, *Carbon*, 2012, **50**, 1538–1545.
- 3 M. Li, S. Hachiya, Z. Chen, T. Osawa, H. Sugime and S. Noda, *Carbon*, 2021, **182**, 23–31.
- 4 J. De La Verpilliere, S. Jessl, K. Saeed, C. Ducati, M. De Volder and A. Boies, *Nanoscale*, 2018, **10**, 7780–7791.
- 5 A. Pander, K. Takano, A. Hatta, M. Nakajima and H. Furuta, *Opt. Express*, 2020, **28**, 607–625.
- 6 H. Miyaji, A. Pander, K. Takano, H. Kohno, A. Hatta, M. Nakajima and H. Furuta, *Diamond Relat. Mater.*, 2018, **83**, 196–203.
- 7 D. He, M. Bozlar, M. Genestoux and J. Bai, *Carbon*, 2010, **48**, 1159–1170.
- 8 S.-Y. Park, W.-D. Kim, D.-G. Kim, J.-K. Kim, Y.-S. Jeong, J. H. Kim, J. K. Lee, S. H. Kim and J.-W. Kang, *Sol. Energy Mater. Sol. Cells*, 2010, **94**, 750–754.
- 9 Y. Piao, K. An, J. Kim, T. Yu and T. Hyeon, *J. Mater. Chem.*, 2006, **16**, 2984–2989.
- 10 D. Y. Kim, H. Sugime, K. Hasegawa, T. Osawa and S. Noda, *Carbon*, 2011, **49**, 1972–1979.
- 11 C. Jo, A. S. Groombridge, J. De La Verpilliere, J. T. Lee, Y. Son, H.-L. Liang, A. M. Boies and M. De Volder, *ACS Nano*, 2020, **14**, 698–707.
- 12 F. S. Boi, G. Mountjoy and M. Baxendale, *Carbon*, 2013, **64**, 516–526.
- 13 T. Chen, B. Cheng, G. Zhu, R. Chen, Y. Hu, L. Ma, H. Lv, Y. Wang, J. Liang, Z. Tie, Z. Jin and J. Liu, *Nano Lett.*, 2017, **17**, 437–444.
- 14 A. B. D. Nandiyanto, Y. Kaihatsu, F. Iskandar and K. Okuyama, *Mater. Lett.*, 2009, **63**, 1847–1850.
- 15 P. Wang and K. Kobiro, *Pure Appl. Chem.*, 2014, **86**, 785–800.
- 16 E. K. C. Pradeep, M. Ohtani, T. Kawaharamura and K. Kobiro, *Chem. Lett.*, 2017, **46**, 940–943.
- 17 P. Wang and K. Kobiro, *Chem. Lett.*, 2012, **41**, 264–266.
- 18 P. Wang, H. Takigawa, K. Ueno and K. Kobiro, *J. Supercrit. Fluids*, 2013, **78**, 124–131.
- 19 K. Kan, E. Yamamoto, M. Ohtani and K. Kobiro, *Eur. J. Inorg. Chem.*, 2020, 4435–4441.
- 20 Y. Kumabe, H. Taga, K. Kan, M. Ohtani and K. Kobiro, *RSC Adv.*, 2020, **10**, 14630–14636.
- 21 A. Taniguchi, R. Miyata, M. Ohtani and K. Kobiro, *RSC Adv.*, 2022, **12**, 22902–22910.
- 22 A. Taniguchi, Y. Kumabe, K. Kan, M. Ohtani and K. Kobiro, *RSC Adv.*, 2021, **11**, 5609–5617.
- 23 E. K. C. Pradeep, M. Ohtani and K. Kobiro, *Eur. J. Inorg. Chem.*, 2015, 5621–5627.
- 24 H. T. T. Nguyen, T. Habu, M. Ohtani and K. Kobiro, *Eur. J. Inorg. Chem.*, 2017, 3017–3023.
- 25 Y. Tanaka, H. Usui, Y. Domi, M. Ohtani, K. Kobiro and H. Sakaguchi, *ACS Appl. Energy Mater.*, 2019, **2**, 636–643.
- 26 M. Meiliefiana, T. Nakayashiki, E. Yamamoto, H. Hayashi, M. Ohtani and K. Kobiro, *Nanoscale Res. Lett.*, 2022, **17**, 47.
- 27 E. K. C. Pradeep, T. Habu, H. Tooriyama, M. Ohtani and K. Kobiro, *J. Supercrit. Fluids*, 2015, **97**, 217–223.
- 28 M. Ohtani, T. Muraoka, Y. Okimoto and K. Kobiro, *Inorg. Chem.*, 2017, **56**, 11546–11551.
- 29 <https://www.ujiden-net.co.jp/marimo/>, accessed Feb 05, 2023.
- 30 F. Duriyasart, A. Irizawa, K. Hayashi, M. Ohtani and K. Kobiro, *ChemCatChem*, 2018, **10**, 3392–3396.
- 31 X. Song, F. Shao, Z. Zhao, X. Li, Z. Wei and J. Wang, *ACS Catal.*, 2022, **12**, 14846–14855.
- 32 A. Jorio and R. Saito, *J. Appl. Phys.*, 2021, **129**, 021102.
- 33 A. C. Ferrari and J. Robertson, *Phys. Rev. B: Condens. Matter Mater. Phys.*, 2000, **61**, 14095–14107.
- 34 M. S. Dresselhaus, G. Dresselhaus, R. Saito and A. Jorio, *Phys. Rep.*, 2005, **409**, 47–99.

